

# Influence Vectors Control for Robots Using Cellular-like Binary Actuators

Alexandre Girard and Jean-Sébastien Plante

**Abstract**—Robots using cellular-like redundant binary actuators could outmatch electric-gearmotor robotic systems in terms of reliability, force-to-weight ratio and cost. This paper presents a robust fault tolerant control scheme that is designed to meet the control challenges encountered by such robots, i.e., discrete actuator inputs, complex system modeling and cross-coupling between actuators. In the proposed scheme, a desired vectorial system output, such as a position or a force, is commanded by recruiting actuators based on their influence vectors on the output. No analytical model of the system is needed; influence vectors are identified experimentally by sequentially activating each actuator. For position control tasks, the controller uses a probabilistic approach and a genetic algorithm to determine an optimal combination of actuators to recruit. For motion control tasks, the controller uses a sliding mode approach and independent recruiting decision for each actuator. Experimental results on a four degrees of freedom binary manipulator with twenty actuators confirm the method's effectiveness, and its ability to tolerate massive perturbations and numerous actuator failures.

## I. INTRODUCTION

ROBOTICS evolved mainly around the one electric gear-motor per joint paradigm. Today's robots are fast and accurate for positioning tasks, such as painting and welding in the automotive industry. However, modern industrial robotic systems still display limited performances in terms of interaction tasks with uncertain environments, because of their high inertia and stiff position-controlled actuators [1]. A radical change in actuation technology and robot architecture is needed to bring robots to a next level and democratize their uses for a wider set of tasks at lower costs.

Soft robots, made of a flexible structure replacing complex components (seals, bearings, gears, motors, etc.), possess the inherent advantages of lightness and compliance and could become a new class of affordable robots [2]. This paper proposes a biologically-inspired actuation architecture where several small active elements, i.e., cellular-like actuators, are embedded in the soft robot body. Many emerging actuator technologies could enable cellular architectures due to their high force to weight ratio and their ability to be embedded

in soft structures: air-muscles [2] [3], dielectric actuators [4] [5], piezoelectric actuators [6], bio-artificial muscles [7] and shape memory alloys actuators [8] [9] [10]. Air-muscles are particularly interesting because the technology is mature and because the stress-strain characteristics of these actuators are in the human motion range and thus no complex reduction/amplification mechanisms are needed. Fig. 1 illustrates a soft pneumatic robot concept where the robot consists of a soft polymer body with a large number of cavities acting as pneumatic actuators.

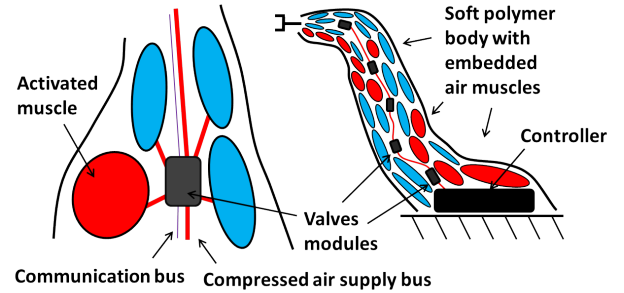


Fig. 1. Soft cellular robot concept with pneumatic actuators.

Soft cellular robots would have many advantages over traditional systems. First, in terms of reliability, such robots would be impact tolerant due to the structure flexibility and the absence of moving parts, and also fault tolerant due to actuators' redundancy. Moreover, they would be lightweight since actuators would share a common structure with the robot body. Furthermore, these robots would be safe for human-machine interaction because of the low impedance of the actuators and structures. Finally, such robots could exhibit very low production costs due to their small number of parts with no need for close tolerance manufacturing as would be required with seals, bearings and gears. Fig. 2 shows a soft exploration robot concept to illustrate new opportunities arising from the proposed soft cellular architecture. Tolerance towards impacts and actuator failures would be a major advantage. An all-polymer robot could fall in canyons and remain functional, even with a few broken air-muscles, a characteristic not possible with current exploration rovers. Moreover, a monopropellant source could be used to power air-muscles [11], as well as thrusters for hopping motions.

Control strategies are a major challenge for robots using cellular-like redundant actuators. With the aim of using a very large number of redundant actuators, each actuator must be simple, lightweight, cheap and miniaturizable. This is why binary (ON/OFF) control is relevant; no low-level control loop is needed and the control hardware can be greatly simplified

This work was supported by the Natural Sciences and Engineering Research Council of Canada (NSERC), the Fonds québécois de la recherche sur la nature et les technologies (FQRNT) and Festo that supplied the pneumatic equipment.

A. Girard and J.-S. Plante are with the Department of Mechanical Engineering, Université de Sherbrooke, Qc, Canada.

<sup>1</sup> ©IEEE. Personal use of this material is permitted. Permission from IEEE must be obtained for all other uses, in any current or future media, including reprinting/republishing this material for advertising or promotional purposes, creating new collective works, for resale or redistribution to servers or lists, or reuse of any copyrighted component of this work in other works. DOI:10.1109/TRO.2013.2296104



Fig. 2. Soft exploration robots.

[12]. For pneumatic robots, low-level control loops are individual pressure-control loops on each actuators, unnecessary with binary control. However, classical continuous control techniques cannot be used directly as the control signal is not continuous. Moreover, with soft embedded structures (see Fig. 1), it is hard to develop analytical models that accurately describe the robot behavior and it is not possible to use independent controllers on each DOF (degrees of freedom), because each actuator is cross-coupled in the sense that each actuator influences more than one DOF.

#### A. Background

Most literature on binary systems control aims at high-repeatability open-loop robots with perfectly constrained systems (one actuator per DOF), unlike the proposed soft cellular-like architecture [12] [13] [14]. An interesting approach, proposed for correcting small mirror deformations using binary actuators [15], uses the superposition principle to compute linear approximations of multiple binary actuators effect by adding their individual effect, thus reducing the needed configuration evaluations from  $2^m$  to  $m$  where  $m$  is the number of binary actuators. Although enlightening, these works focused on open-loop strategies that are limited when it comes to control soft robots that cannot be modeled accurately. Open-loop control is also problematic because of inevitable manufacturing errors and hysteresis behaviors [16] [17]. Hence, a global closed-loop approach is deemed necessary to reject model uncertainties and external perturbations for the control of soft cellular-like robots.

A closed-loop technique called *broadcast feedback* was developed for binary cellular-like actuators [18]. Although very promising, this technique is aimed at huge numbers (1000+) of actuators and is developed for single output systems only. Another closed-loop control technique for binary systems was proposed for actuators that behave like force sources [19]. It has been shown effective on a single DOF system using 25 identical pneumatic actuators, and also tolerant to actuator failures in a similar experiment [20]. This technique needs a nodes-elements mathematical description of the system that can hardly be constructed for soft robots. To date, there is no binary control scheme to handle cross-coupled multi-DOF systems without analytical models.

#### B. Approach and Results

This paper presents a closed-loop control scheme for multi-DOF binary systems based on the concept of influence vectors (section II) and verifies its effectiveness experimentally on a soft polymer binary robot (section III). A static scheme addresses point-to-point tasks, i.e., position control, while a dynamic scheme addresses tracking tasks, i.e., motion control. The work extends a previous preliminary demonstration [21], by bringing a formal presentation and exhaustive experimental results. Results show the influence vectors approach to be effective and able to tolerate massive perturbations and numerous actuator failures.

## II. PROPOSED CONTROL SCHEME

#### A. Influence Vectors

Each influence vector is a vectorial quantity, such as a displacement or a force, resulting from the action of an individual actuator. Influence vectors are identified during an initial start-up calibration where the robot sequentially activates each actuator. The set of influence vectors forms an experimental input-output model to predict the evolution of the system for given actuation commands, using linear approximations computed with the superposition principle.

For the static scheme, a state vector  $\mathbf{x}$  describing the controlled DOFs of the system output is chosen, such as the end-effector displacement for a robot manipulator (see Fig. 3). The influence vectors  $\mathbf{d}_k$  are then the individual steady-state effects, on the state vector  $\mathbf{x}$ , of each binary actuators  $k$ :

$$\mathbf{d}_k = \mathbf{x}_k - \mathbf{x}_0 \quad (1)$$

where  $\mathbf{x}_k$  is the state vector when only actuator  $k$  is on and  $\mathbf{x}_0$  is the state vector when all actuators are off.

For the dynamic scheme, the influence vectors consists of the corresponding force quantities  $\mathbf{f}_k$  when all DOFs are constrained (see Fig. 3). Although possible, it is not always practical to experimentally evaluate the force vectors  $\mathbf{f}_k$  directly. In such cases, displacement influence vectors  $\mathbf{d}_k$  of a system can be related to their force vectors  $\mathbf{f}_k$  by a stiffness matrix ( $\mathbf{f}_k = \mathbf{K} \mathbf{d}_k$ ), assuming a linear system. Though this implies knowing or having to evaluate the system stiffness  $\mathbf{K}$ .

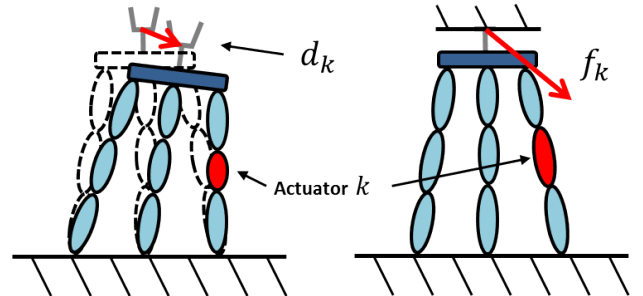


Fig. 3. Influence vectors for a planar manipulator: left, a displacement influence vector and, right, a force influence vector.

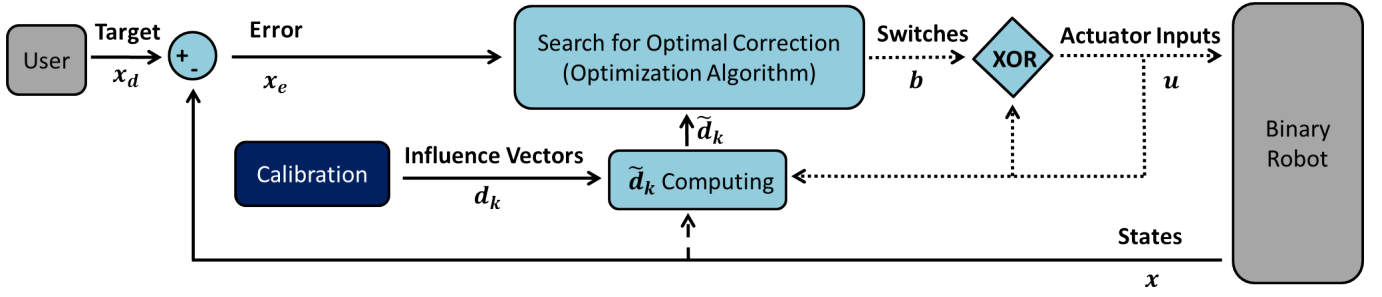


Fig. 4. Static control scheme, dotted lines are for binary vectors (i.e., vectors of 0's and 1's) and the dashed line is an optional feedback linearization loop.

### B. Static Control

This section presents a control technique for point-to-point control, i.e., when only the final position is important and not the path taken. This scheme is called static control because actuator inputs  $u$  are only changed after the robot reached a steady state. Fig. 4 illustrates the static control scheme where an algorithm searches an optimal combination of binary actuators to recruit, i.e., a switch vector  $b$ , in order to correct the static state error defined as :

$$x_e = x_d - x \quad (2)$$

where  $x$  is the state vector and  $x_d$  the desired state vector.

The system evolution, from one steady state to another, is described by a set of difference equations:

$$x(n+1) = x(n) + \Delta x \quad (3)$$

$$u(n+1) = b \oplus u(n) \quad (4)$$

where  $u$  is the actuator input vector and  $b$  is the switch vector used to command actuators input changes (XOR operator).

First, influence vectors  $d_k$  must be updated at each step to account for current actuator input state. For instance, when an actuator is already ON, the only possible action is going back to the OFF state. Hence, updated influence vectors  $\tilde{d}_k$  are given by:

$$\tilde{d}_k(u_k) = \begin{cases} +d_k & \text{if } u_k = 0 \\ -d_k & \text{if } u_k = 1 \end{cases} \quad (5)$$

If the system is fully linear, updated influence vectors are the same everywhere in the state space of the system and independent of other actuator inputs. If the system has some non-linearities, the influence vectors could be corrected using the state vector and the actuation inputs vector, i.e.,  $\tilde{d}_k = f(u, x)$ . This correction would be similar to feedback linearization in classic control and is illustrated by the dashed line on Fig. 4.

With the updated influence vectors  $\tilde{d}_k$ , it is now possible to compute a first order linear approximation  $a$  of the state changes  $\Delta x$  for a given switch vector  $b$ , using the superposition principle:

$$\Delta x \approx a(b) = \sum b_k \tilde{d}_k \quad (6)$$

Using a linear algebra form, eq. (6) becomes:

$$a = Jb \quad \text{with} \quad J = [\tilde{d}_1 \dots \tilde{d}_k \dots \tilde{d}_m] \quad (7)$$

Hence, system evolution is predicted by:

$$x(n+1) \approx x(n) + Jb \quad (8)$$

The matrix  $J$ , constructed with all the updated influence vectors  $\tilde{d}_k$ , is the Jacobian matrix of the state vector  $x$  over the switch vector  $b$ . The influence vectors can thus be interpreted as an experimental evaluation of this Jacobian matrix around  $x = 0$  and  $u = 0$ .

The controller, however, needs to solve the inverse problem: to find a switch vector  $b$  that will create a state change  $\Delta x$  equal to the static error  $x_e$ . Hence, if  $b$  was a regular vector it would be computed from:

$$b = J^{-1} x_e \quad (9)$$

and there would be an infinite number of solution since there is more actuators then controlled states. However  $b$  is a binary vector, i.e., each of its element can only take a value of 0 or 1, and the solution set is discrete and finite ( $2^m$  possible  $b$  vector where  $m$  is the number of actuators). Hence, there is no exact solution. Instead, a solution is computed by minimizing a cost function defined as the norm of the resolution error  $\epsilon_r$  :

$$\epsilon_r = Jb - x_e \quad (10)$$

The forward solution space needs to be explored using a search algorithm in order to minimize the cost function under the binary constraint of  $b$ . An exhaustive search becomes too computer intensive when the number of actuators gets higher than about 12. Fortunately, when the number of actuators is large, there are many good enough solutions and an optimization algorithm can find one quickly. Different algorithms have been proposed for binary solution optimization, such as genetic algorithms [14] and neural networks [19]. Algorithm selection is application dependant and one designed for the experimental platform used in this paper is presented in section III-B.

The error correction process uses local linear approximations and is thus not perfect. Therefore, corrections are performed iteratively until the error becomes acceptable. Moreover, the iterative process makes the static scheme behave like an integral action; if an error is persistent, then at each iteration, the controller will recruit more actuators to fight it until all useful actuators have been recruited. This makes the controller robust to perturbations and actuators failures. The major drawback of the static scheme is the fact of having to wait for the stabilization of the states between each iterative correction.

### C. Approximation Error and Convergence

Controller iterations will converge as long as the linear approximation  $a$  remains a good approximation of the sys-

tem behavior. For highly non-linear systems, the feedback linearization loop  $\tilde{d}_k(u, x)$  might be necessary to keep the approximations pointing in the right direction to ensure convergence. The basins of attraction for such methods remain to be studied.

Without a stopping criterion, the controller can enter limit cycles when the robot gets close to the target. This happens when the error  $x_e$ , and thus computed corrections, gets in the range of the approximation error  $\epsilon_a$ , defined as the difference between the effective state change  $\Delta x$  and the approximation  $a$  such that :

$$\Delta x = x(n+1) - x(n) = a + \epsilon_a \quad (11)$$

As shown in Fig. 5, the next state error  $x_e(n+1)$  will then be equal to :

$$x_e(n+1) = x_d - x(n+1) = -(\epsilon_r + \epsilon_a) \quad (12)$$

In order to guarantee convergence, the norm of the sum of both errors must be bounded and inferior to the norm of the actual state error:

$$\|\epsilon_r + \epsilon_a\|_{max} < \|x_e(n)\| \quad (13)$$

The resolution error  $\epsilon_r$  is known from the result of the search algorithm. Thus, if the approximation error  $\epsilon_a$  can be bounded, a region can be defined in the state space where  $x(n+1)$  is guaranteed to be in (see Fig. 5). If every point of this zone is closer to the target  $x_d$  than the actual state  $x(n)$ , convergence of the next iteration is guaranteed.

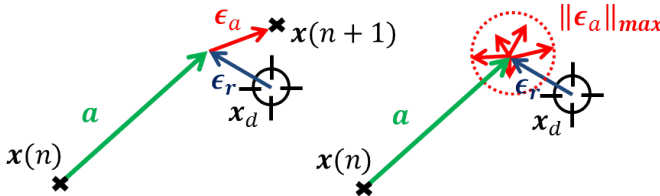


Fig. 5. Resolution error vector  $\epsilon_r$  and approximation error vector  $\epsilon_a$ .

A fixed upper bound  $\|\epsilon_a\|_{max}$  on approximation errors can be set either theoretically or experimentally. Alternatively, a probabilistic assessment of the system evolution could lead to greater accuracy by being less severe on the criterion guaranteeing convergence. Instead of an upper bound  $\|\epsilon_a\|_{max}$ , the standard deviation of the approximation error  $\sigma_\epsilon$  is used as the measure of dispersion. The convergence probability is then evaluated and used as a stopping criterion:

$$P_{conv} = P(\|\epsilon_r + \epsilon_a\| < \|x_e(n)\|) \quad (14)$$

The convergence probability can be computed using a noncentral chi-squared distribution, assuming independent and normal distributions of the approximation error on each DOF.

#### D. Probabilistic Cost Function

Approximation errors  $\epsilon_a$  are greater for corrections involving many actuators due to error addition and because linear approximations  $a$  do not account for higher order coupling effects. This section presents a probabilistic approach

to minimize simultaneously the resolution error  $\epsilon_r$  and the approximation error  $\epsilon_a$ , by prioritizing solutions with low number of switching actuators.

First, the measure of approximation error dispersion, i.e., the standard deviation  $\sigma_\epsilon$ , should be identified as a function of the number of switching actuators. This can be done by identifying the individual dispersion contribution of each actuators  $\sigma_{\epsilon,k}$ . Assuming independent error sources, the total dispersion for a given switch vector  $b$  is then given by:

$$\sigma_\epsilon^2 = \sum b_k \sigma_{\epsilon,k}^2 \quad (15)$$

If the individual error contributions  $\sigma_{\epsilon,k}$  are all equal, the total dispersion is given by:

$$\sigma_\epsilon = \sqrt{s_n} \sigma \quad \text{if } \sigma_{\epsilon,k} = \sigma \forall k \quad (16)$$

where  $s_n$  is the number of switching actuators ( $s_n = \sum b_k$ ).

Second, a new probabilistic cost function is defined for the optimization algorithm. A target zone, centered on the desired states  $x_d$  and bounded by allowable errors  $\epsilon_{d,i}$ , is specified, see Fig. 6. The cost function is then defined as the inverse of the probability of arriving in this zone, instead of the norm of the resolution error  $\epsilon_r$ .

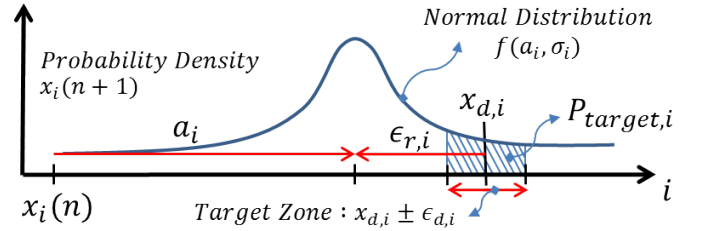


Fig. 6. Probability of arriving in the target zone for one DOF.

The approximation  $a$  gives the expected value and the vector  $\sigma_\epsilon$ , computed with eq. (15) or eq. (16), gives the predicted standard deviation. Assuming normal error distributions, the probabilities  $P_{target,i}$  to arrive in the target zone for each DOF  $i$  can be computed with standard error functions.

For multiple DOFs, the overall on-target probability  $P_{target}$ , i.e., the probability to be in the target zone on all DOFs, is the multiplication of all individual probabilities, assuming independent error distributions on each DOF :

$$P_{target} = \prod P_{target,i} \quad (17)$$

$$P_{target} = \prod P(-\epsilon_{d,i} < \epsilon_{r,i} + \epsilon_{a,i} < \epsilon_{d,i}) \quad (18)$$

Using the probabilistic cost function, the controller algorithm will, not only optimize the accuracy of the correction, i.e.,  $\epsilon_r$ , but also the precision of the correction, i.e.,  $\sigma_\epsilon$ .

Fig. 7 illustrates the behavior of the probability density function for one DOF. Case A illustrates a solution with a low resolution error  $\epsilon_r$  but using many actuators thus creating high uncertainty while case B illustrates a solution with a slightly bigger resolution error  $\epsilon_r$  but less uncertainty due to a low number of switching actuators. The best solution is the one with the bigger area under the probability density curve for the specified target zone.



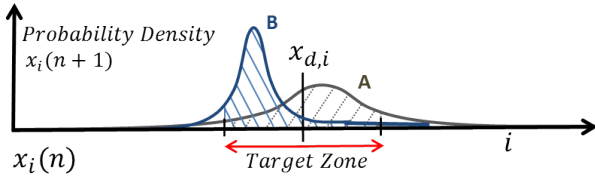


Fig. 7. Probability density curves of two possible solutions on one DOF. Case A : a high accuracy but low precision solution (many actuators switching), Case B : a low accuracy but high precision solution (few actuators switching).

In practice, including the precision in the cost function of the optimization algorithm means that the controller will prioritize solutions recruiting small number of actuators. The minimization of the switching activity also has other positive effects such as reducing energy consumption and mechanical cycling of the system.

#### E. Dynamic Control

Here, a highly robust controller is proposed in the form of a simple bang-bang sliding mode controller. The composite vector  $s$  is computed as a weighted sum of the state error vector and its derivative:

$$s = \dot{x}_e + \lambda x_e \quad (19)$$

Actuators are now seen as force sources instead of displacement sources and the control law that force  $s$  to zero, assuming that actuator force vectors  $\mathbf{f}_k$  are numerous and diverse, is:

$$b_k = \begin{cases} 1 & \text{if } \text{sgn}(s \bullet \tilde{\mathbf{f}}_k) > 0 \\ 0 & \text{if } \text{sgn}(s \bullet \tilde{\mathbf{f}}_k) \leq 0 \end{cases} \quad \forall k \quad (20)$$

Then, keeping  $s$  near zero will impose a first order convergence for the error  $x_e$ , with a time constant adjusted by the value of the  $\lambda$  parameter. This bang-bang controller is particularly interesting because it eliminates the need for computation-heavy search algorithms that can be hard to implement in real-time controllers. The control law is simple: the controller checks each actuator to know if their updated force influence vectors  $\tilde{\mathbf{f}}_k$  points in the direction of the composite error vector  $s$ ; if so the actuator is recruited. With this bang-bang law, only the directions of the influence vectors matters. Hence, if the system is isotropic, the updated displacement influence vectors  $\tilde{\mathbf{d}}_k$  can be used directly without a conversion to force requiring a stiffness matrix  $\mathbf{K}$ . Moreover, since the decision to switch input states is independent for each actuator, it would be possible to broadcast the error vector to decentralized mini-controllers on each actuator like previously proposed for single output systems [18].

### III. EXPERIMENTAL VALIDATIONS

#### A. Binary Robot Prototype

The proposed static and dynamic controllers based on influence vectors are tested on a soft polymer robot actuated by twenty binary air muscles, see Fig. 8. This robot is designed to orient a needle guide inside a magnetic resonance imaging system for accurate medical interventions [22]. The robot has

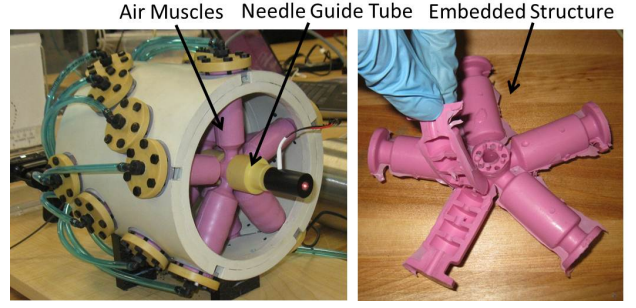


Fig. 8. Soft polymer robot prototype using embedded air-muscles [22].

four actuated DOFs, two rotations and two translations. The experimental set-up uses two lasers to project the axis of the needle guide on two planes (see Fig. 9). Two cameras capture the positions of the laser dots. Each actuator is connected to a solenoid valve (*Festo VUVG*) that connects the muscle either to the atmosphere or to a two-liter reservoir regulated at 32 PSI by a proportional valve.

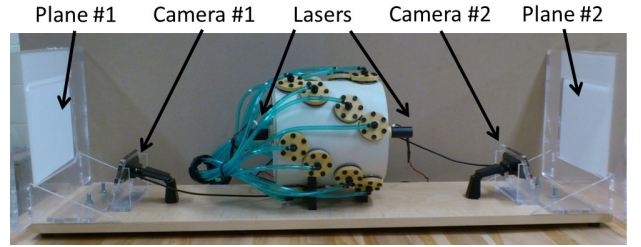


Fig. 9. Experimental Set-up.

#### B. Controller Implementation

The control algorithm is implemented in a *Python* script running under *Windows 7* on a *Intel Core i3* laptop. A *labjack u3* card handles I/O and a microcontroller converts the output vector  $\mathbf{u}$  from a digital signal to 20 analog outputs.

1) *State Sensing*: Camera images are processed using *OpenCV* functions to find the centroid of the laser dots. The acquisition and computing time is about 0.2 sec and the resolution on the displacement is about 0.2 mm. Camera coordinates are then transformed to real-world coordinates using a perspective projection, using camera parameters computed with a chessboard calibration pattern. This analysis outputs the positions of the laser line intersections in both planes,  $\mathbf{p}_1$  and  $\mathbf{p}_2$ , as illustrated on Fig. 10. These two vectors describe 4 DOFs, the rotation and translation along the laser line are unimportant for needle guidance and thus remain unactuated.

The position vectors  $\mathbf{p}_1$  and  $\mathbf{p}_2$  are then transformed into virtual end-effector states in a x-y work plane where the target is located. A vector  $\mathbf{t}$  is defined as the x-y position of the intersection of the laser line with this x-y plane. The rotation  $\mathbf{R}$  of the laser line is defined as the unit rotation axis vector multiplied by the rotation angle. The rotation vector  $\mathbf{R}$  is computed with respect with the z axis and is thus always in a x-y plane. Since both vectors  $\mathbf{t}$  and  $\mathbf{R}$  are located in a x-y

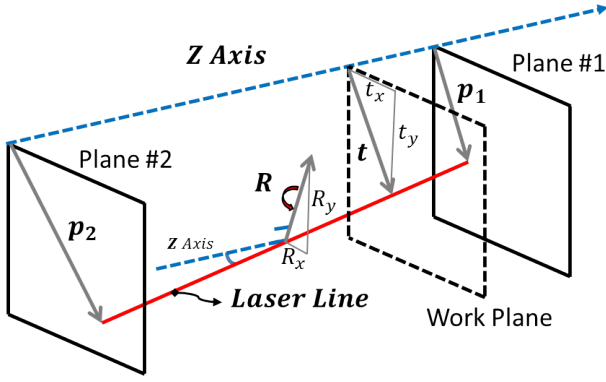


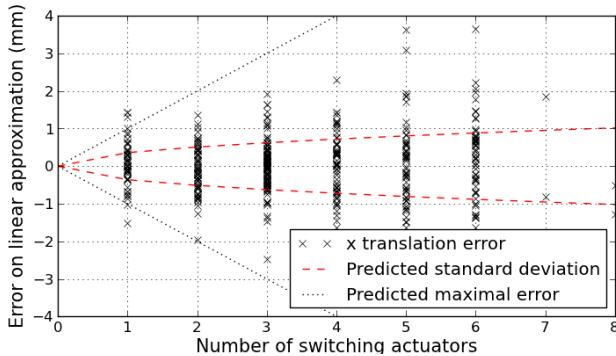
Fig. 10. Kinematic of the robot.

plane, the state vector describing the end effector position can be defined with 4 DOFs:

$$\mathbf{x} = \begin{bmatrix} \mathbf{t} \\ \mathbf{R} \end{bmatrix} = \begin{bmatrix} t_x \\ t_y \\ R_x \\ R_y \end{bmatrix} \quad (21)$$

For all experiments presented in this paper the work plane  $z$  coordinate was set to coincide with plane #1.

2) *Error Distribution*: The approximation error  $\epsilon_a$  distribution was experimentally evaluated for a hundred random corrections. As expected, the error increases with the number of switching actuators, as illustrated by Fig. 11 showing the approximation error in function of the number of switching actuators. Also, the error is found to be uncorrelated with the following factors: distance to base point where influence vectors are evaluated, number of already ON actuators and motion directions. Furthermore, the contribution to the error of each actuator shows no significant variations from one to another. It was therefore possible to characterize the approximation error as a random variable function of the number of switching actuators only. The standard deviation of the error  $\sigma_\epsilon$  on each degree of freedom is computed from the experimental sample, and found to be about  $0.35\sqrt{s_n}$  mm on  $t_x$  and  $t_y$  and  $0.025\sqrt{s_n}$  degrees on  $R_x$  and  $R_y$ , where  $s_n$  is the number of switching actuators.

Fig. 11. Approximation error on  $t_x$  in function of the number of switching actuators.

3) *Cost Function*: The cost function defines the value of a given switch vector  $\mathbf{b}$  for a given situation, i.e., an error vector  $\mathbf{x}_e$  and available influence vectors  $\tilde{\mathbf{d}}_k$ . Three cost functions were evaluated: the norm of the resolution error  $\|\epsilon_r\|$ , the inverse of the on-target probability  $1/P_{target}$  and the norm of the resolution error plus a penalty proportional to the number of switching actuators  $\|\epsilon_r\| + 0.2s_n$ . Moreover, independant weight for each DOF can be set. For instance, if it is desired to achieve the best possible in-plane translation  $\mathbf{t}$  accuracy without any consideration for the needle-guide orientation  $\mathbf{R}$ , then both  $R_x$  and  $R_y$  weights can be set to zero. Such cases are referred as translation-only targets. The 3 cost functions are experimentally evaluated on the prototype for 3 static translation-only targets. TABLE I shows the mean results of 3 tests per target,  $\epsilon$  is the final absolute translation error and  $n_f$  is the number of iterations used. A significant performance improvement is found for the two cost functions penalizing the number of switching actuators. However, no difference is found between the probabilistic cost function and the simplified proportional version. Hence, it is the simplified cost function that is used in the remaining experiments since its evaluation is faster than the evaluation of the probabilistic cost function.

	Target #1		Target #2		Target #3	
Cost Function	$n_f$	$\epsilon$	$n_f$	$\epsilon$	$n_f$	$\epsilon$
$\ \epsilon_r\ $	5	0.5 mm	4	0.9 mm	4	0.9 mm
$1/P_{target}$	3	0.5 mm	1	0.3 mm	3	0.4 mm
$\ \epsilon_r\  + 0.2s_n$	3	0.5 mm	1	0.3 mm	3	0.4 mm

TABLE I  
COST FUNCTIONS EXPERIMENTAL EVALUATION

4) *Optimization Algorithm*: The optimization algorithm that finds a switch vector  $\mathbf{b}$  minimizing the cost function during each iteration loop is shown in Fig. 12. The algorithm optimizes a solution in about 0.3 sec, which is acceptable since the bandwidth bottleneck of the static controller is a three seconds delay imposed between each iterations to let the robot reach a steady state between each correction.

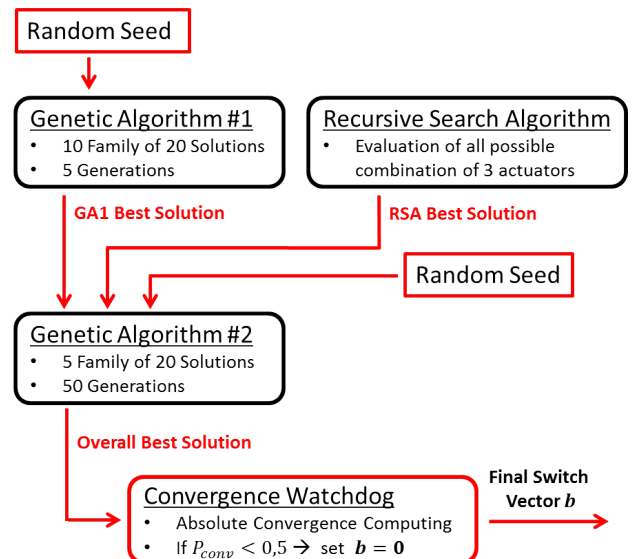


Fig. 12. Implemented optimization algorithm.

Since a good solution has a low number of switching actuators, all solutions that switch only three or less actuators are evaluated first. In parallel, a widespread, i.e., many members and few generations, genetic algorithm optimizes a solution. The best solutions of those two searches are then inserted in the population of another genetic algorithm with fewer members but many generations that complete the optimization more locally. The random seeds of both genetic algorithm are randomly generated binary switch vectors  $\mathbf{b}$  with four switching actuators or more. For the selection step, the *roulette-wheel selection* method is used. For the crossing step, segments of 5 bits are randomly exchanged between solutions, with a probability of 0.1 for each bit to be the base of a crossing. Then, for the mutation step, a switching probability of 0.025 is used for each bit. The algorithm performances are however subject to improvement as the focus of this work was not put on the optimization of the algorithmic aspect.

### C. Static Controller Results

To evaluate the static controller, the same three randomly-selected targets are used for all static controller experiments. Also, a three-second delay is imposed to let the robot stabilize to a steady state between each correction. Typical performance of the static controller is shown on Fig. 13 for translation-only targets, on Fig. 14 for rotation-only targets and on Fig. 15 for simultaneous translation and rotation targets.

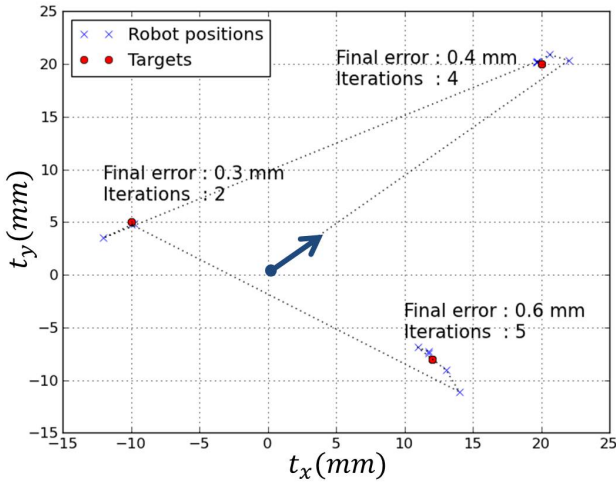


Fig. 13. Static control results for translation-only targets.

The static controller performs well for controlling two DOFs while letting two free. Sub-millimeter accuracy, almost at the resolution limit of the cameras, is reached with on average 4 iterations for translation-only targets. The accuracy is lower, in the order of 1-2 mm, see Fig. 15, for the simultaneous control of the four DOFs. This limited performance is explained by the limited discrete workspace of the 20 actuators binary robots. Ten bits are available per DOF which means 1024 discrete positions per DOF when two DOFs are controlled. Five bits are available per DOF which means only 32 discrete positions per DOF when all four DOFs are controlled. This problem can

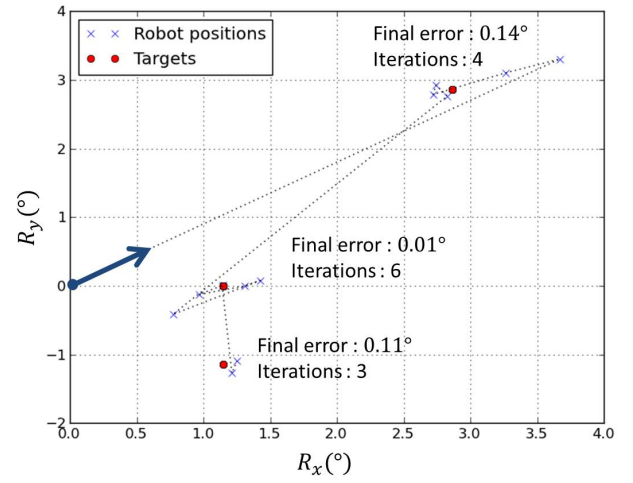


Fig. 14. Static control results for rotation-only targets.

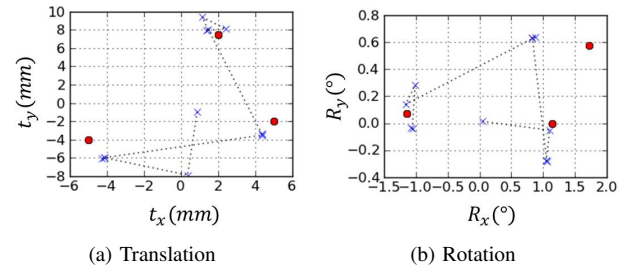


Fig. 15. Static control results for simultaneous control of translation and rotation.

be addressed by using systems with more binary actuators. Adding only a few actuators would drastically improve the resolution since the relation is exponential. The rest of this paper presents experiments with translation-only targets.

Fig. 16 show the controller's ability to reject perturbations caused by a load that was attached to the robot after the third iteration. The controller is able to correct the perturbation-induced error and system performance is not affected for the following targets even though the load is still on the robot.

Fig. 17 shows the ability of the controller to operate in the event of actuator failures. In this experiment, three valves were intentionally blocked open. Fig. 18 simulates the case where these failures could be detected and accounted for by removing defective actuators from the list of possible actuators to recruit. The robot makes inaccurate moves each time the computed correction uses those actuators for the case with undetected failed actuators, but these errors are corrected by following iterations. Erratic moves stop as soon as failures are detected. However, system resolution diminishes for each out-of-service actuators. Table II shows the results of the controller performances for up to 10 actuator failures out of 20. Since the controller is not determinist (random seeds), corrections chosen and performance may be different for two identical situations. Moreover, for some rare lucky situations it could happen that the unpredictable approximation error  $\epsilon_a$  cancel out the resolution error  $\epsilon_r$ . This is why the presented results should be used with care as the randomness involved can bring

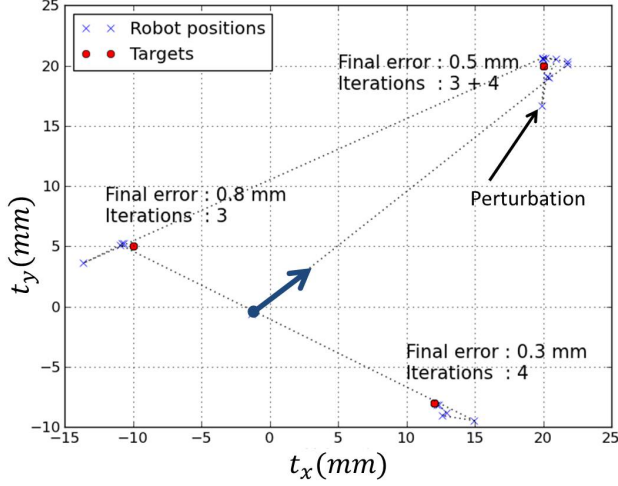


Fig. 16. Static control, with a perturbation applied after three iterations.

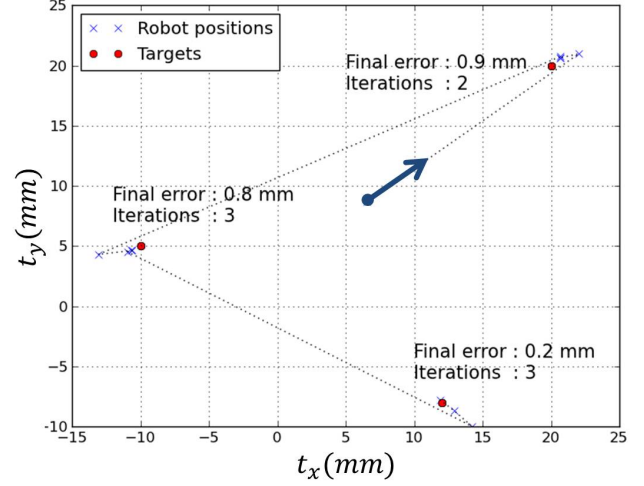


Fig. 18. Static control, with three actuators failures detected.

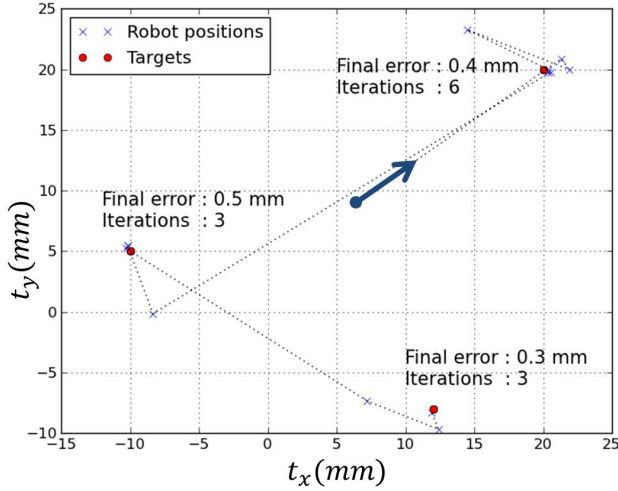


Fig. 17. Static control, with three actuators failures undetected.

odd results, such as the better performance of the controller with 10 actuator failures than none, for target # 1.

Failures	Target #1		Target #2		Target #3	
	$n_f$	$\epsilon$	$n_f$	$\epsilon$	$n_f$	$\epsilon$
None	4	0.4 mm	2	0.3 mm	5	0.6 mm
3	6	0.4 mm	3	0.5 mm	3	0.3 mm
3 detected	2	0.9 mm	3	0.8 mm	3	0.2 mm
6	4	0.9 mm	9	0.7 mm	4	0.4 mm
6 detected	3	0.7 mm	3	0.6 mm	2	0.3 mm
10	2	0.3 mm	9	6.5 mm	9	1.8 mm
10 detected	1	0.2 mm	2	1.4 mm	2	1.7 mm

TABLE II

STATIC CONTROLLER PERFORMANCE WITH ACTUATORS FAILURES

#### D. Dynamic Controller Results

The experimental set-up was not designed for dynamic experiments and was limited to a 5 Hz control bandwidth because of cameras-induced delays. Such limitations are particularly problematic for sliding mode controllers since the

chattering is proportional to control loop delays [23]. Fig. 19 shows results with static targets and Fig. 20 and 21 show results for a trajectory following task. Results show good potential considering the low control loop frequency. Inevitable chattering occurred, with an oscillation amplitude of about 1 mm.

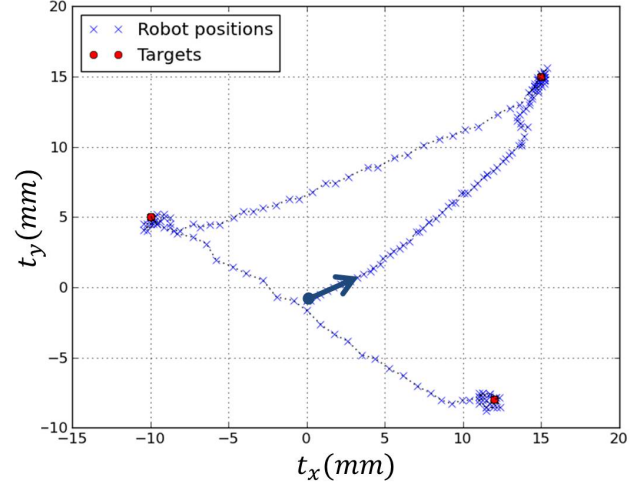


Fig. 19. Dynamic controller with static targets.

Fig. 22, Fig. 23, Fig. 24 and Fig. 25 present tracking results for respectively 4, 7, 10 and 14 blocked valves out of 20 to simulate actuators failures. The proposed bang-bang controller is found to be very robust to actuator failures. In fact, since the control decision is independent for each actuator, the controller itself is insensitive to broken actuators, although failures will physically limit the system. For instance, with 7 and 10 out-of-service actuators (see Fig. 23 and Fig. 24), the robot was still able to track trajectories but could not reach the upper part of the workspace, as too many actuators pushing up were unavailable.



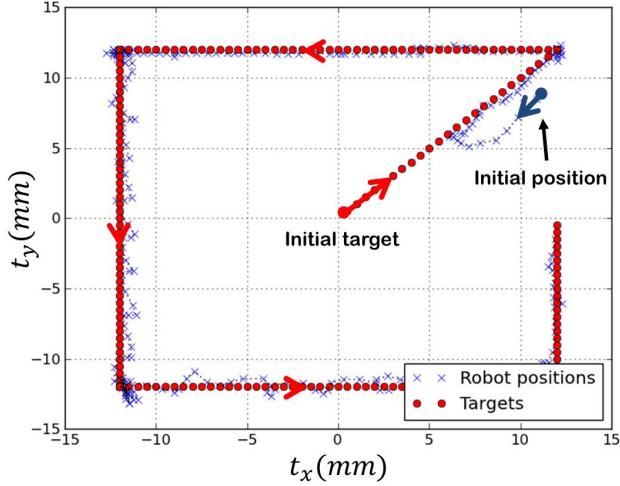


Fig. 20. Dynamic controller with a tracking task.

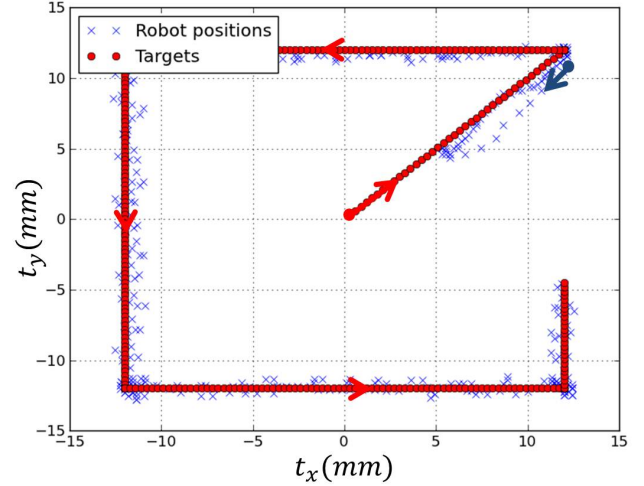


Fig. 22. Dynamic controller with a tracking task with 4 actuators faults.

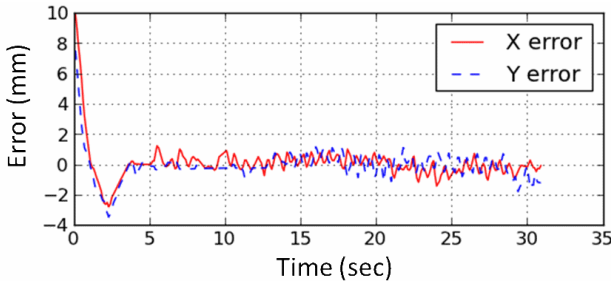


Fig. 21. Tracking error of the dynamic controller.

#### IV. CONCLUSION AND OUTLOOK

In this paper, a closed-loop control scheme that can be used on any binary actuated system that is naturally stable is proposed. No analytical model of the system is needed since the scheme relies on experimentally identified influence vectors. A static iterative controller addresses point-to-point tasks and a dynamic controller addresses motion control tasks. The static controller uses a genetic algorithm that searches for optimal combinations of actuators to recruit, iteratively, in order to correct the system error. Corrections are evaluated using the influence vectors and the superposition principle. Experimental results show the static controller to be effective and robust against perturbations and actuators failures. The dynamic controller determines independently the ON-OFF state of each actuators by comparing the direction of their influence vectors with the direction of a composite error vector. Experimental results show high potential, i.e., motion tracking with robustness to perturbations and actuators failures, despite the limited test bench bandwidth. Future work should however include tests using a real-time set-up to evaluate the full potential of the proposed dynamic controller.

The proposed controllers can be used as a base framework for many future developments of binary or cellular-like robots. For instance, an adaptive scheme could be incorporated where the influence vectors could be identified and calibrated online,

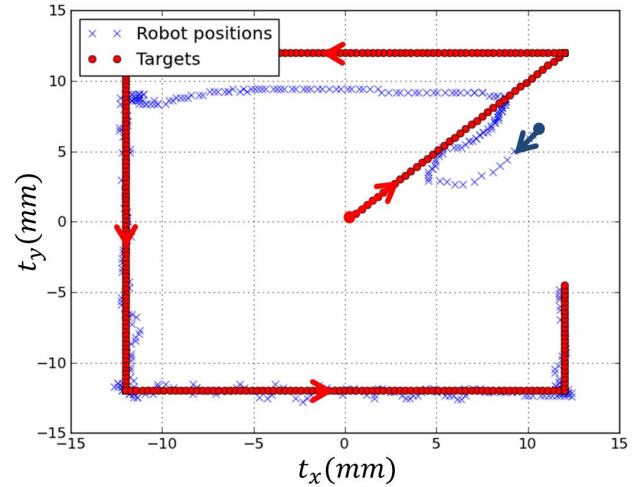


Fig. 23. Dynamic controller with a tracking task with 7 actuators faults.

as well as non-linear behaviors and actuator failures. The influence vectors approach could also be expanded to non-binary robots by adding adjustable amplitudes to the influence vectors. Moreover, it would be interesting to develop a hybrid controller that could switch from the dynamic controller to the static controller to limit control activity when the targets become static. At last, a positive non-zero threshold (see eq. (20)) for the proposed bang-bang controller, that could be stochastic for large numbers of actuators [18], could help moderate the chattering behavior.

#### ACKNOWLEDGMENTS

Special thanks to Geneviève Miron for the robot development, Marc Denninger for the 3D graphic art and Benoit Heintz for the electronics of the experimental set-up.

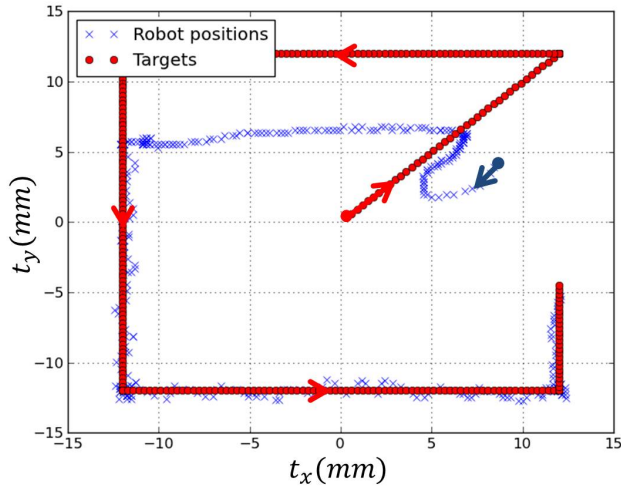


Fig. 24. Dynamic controller with a tracking task with 10 actuators faults.

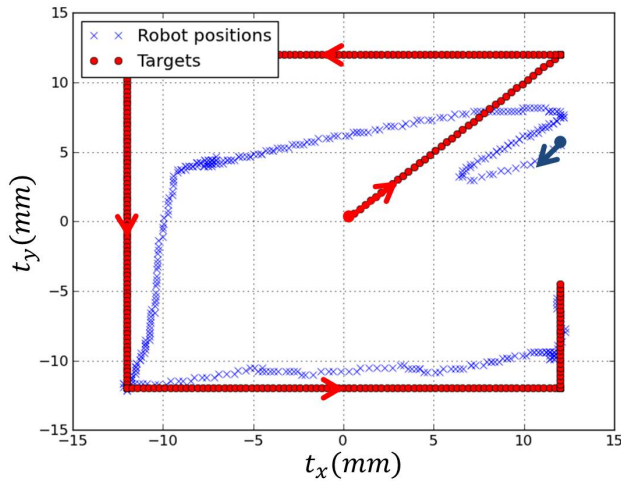


Fig. 25. Dynamic controller with a tracking task with 14 actuators faults.

## REFERENCES

- [1] P. Fauteux, M. Lauria, B. Heintz, and F. Michaud, "Dual-differential rheological actuator for high-performance physical robotic interaction," *IEEE Transactions on Robotics*, vol. 26, no. 4, pp. 607–618, Aug. 2010.
- [2] R. F. Shepherd, F. Ilievski, W. Choi, S. A. Morin, A. A. Stokes, A. D. Mazzeo, X. Chen, M. Wang, and G. M. Whitesides, "Multigait soft robot," *Proceedings of the National Academy of Sciences*, vol. 108, no. 51, pp. 20 400–20 403, Nov. 2011.
- [3] "Bionic handling assistant," 2010. [Online]. Available: [www.festo.com](http://www.festo.com)
- [4] A. Wingert, M. Lichter, and S. Dubowsky, "On the design of large degree-of-freedom digital mechatronic devices based on bistable dielectric elastomer actuators," *IEEE/ASME Transactions on Mechatronics*, vol. 11, no. 4, pp. 448–456, Aug. 2006.
- [5] I. A. Anderson, T. A. Gisby, T. G. McKay, B. M. O'Brien, and E. P. Calius, "Multi-functional dielectric elastomer artificial muscles for soft and smart machines," *Journal of Applied Physics*, vol. 112, no. 4, pp. 041 101–041 101, Aug. 2012.
- [6] J. Ueda, L. Odhner, S.-G. Kim, and H. Asada, "Distributed stochastic control of MEMS-PZT cellular actuators with broadcast feedback," in *International Conference on Biomedical Robotics and Biomechanics*. IEEE/RAS-EMBS, 2006, pp. 272–277.
- [7] D. Neal and H. Asada, "Co-fabrication of live skeletal muscles as actuators in a millimeter scale mechanical system," in *International Conference on Robotics and Automation*. IEEE, May 2011, pp. 3251–3256.
- [8] K.-J. Cho and H. H. Asada, "Architecture design of a multi-axis cellular actuator array using segmented binary control of shape memory alloy," *IEEE Transactions on Robotics*, vol. 22, no. 4, pp. 831–843, Aug. 2006.
- [9] J. Hollerbach, I. Hunter, and J. Ballantyne, "A comparative analysis of actuator technologies for robotics," in *The Robotics Review*, MIT press ed., 1992, vol. 2, pp. 299–342.
- [10] J. D. Madden, N. A. Vandesteeg, P. A. Anquetil, P. G. Madden, A. Takshi, R. Z. Pytel, S. R. Lafontaine, P. A. Wieringa, and I. W. Hunter, "Artificial muscle technology: physical principles and naval prospects," *IEEE Journal of Oceanic Engineering*, vol. 29, no. 3, pp. 706–728, Jul. 2004.
- [11] M. Gogola, E. J. Barth, and M. Goldfarb, "Monopropellant powered actuators for use in autonomous human-scaled robotics," in *International Conference on Robotics and Automation*, vol. 3. IEEE, 2002, pp. 2357–2362.
- [12] M. Lichter, V. Sujun, and S. Dubowsky, "Experimental demonstration of a new design paradigm in space robotics," *7th International Symposium on Experimental Robotics*, pp. 10–13, 2000.
- [13] G. S. Chirikjian, "Binary paradigm for robotic manipulators," in *International Conference on Robotics and Automation*. IEEE, 1994, pp. 3063–3069.
- [14] M. Lichter, V. Sujun, and S. Dubowsky, "Computational issues in the planning and kinematics of binary robots," in *International Conference on Robotics and Automation*, vol. 1. IEEE, 2002, pp. 341–346.
- [15] S. J. Lee, A. M. Bilton, and S. Dubowsky, "On the kinematics of solar mirrors using massively parallel binary actuation," in *International Design Engineering Technical Conferences and Computers and Information in Engineering Conference*, vol. 2. ASME, 2010, pp. 1177–1186.
- [16] S. Proulx and J.-S. Plante, "Design and experimental assessment of an elastically averaged binary manipulator using pneumatic air muscles for magnetic resonance imaging guided prostate interventions," *Journal of Mechanical Design*, vol. 133, no. 11, pp. 111011–111011, 2011.
- [17] K. Kirsch, M. Kean, and R. J. Cipra, "Experimental optimization of a discrete robot exhibiting hysteresis," in *International Design Engineering Technical Conferences & Computers and Information in Engineering Conference*. Chicago, IL, USA: ASME, Aug. 2012, pp. 1115–1124.
- [18] J. Ueda, L. Odhner, and H. Asada, "A broadcast-probability approach to the control of vast DOF cellular actuators," in *International Conference on Robotics and Automation*. IEEE, May 2006, pp. 1456–1461.
- [19] P.-h. Yang and K. J. Waldron, "Massively parallel actuation," in *International Conference on Advanced Intelligent Mechatronics*, vol. 2. IEEE/ASME, 2001, pp. 868–873.
- [20] O. Ramana Murthy, A. Panda, S. Mukherjee, and I. Kar, "Fault tolerant operation of one dimensional MPBS," in *Conference on Convergent Technologies for Asia-Pacific Region*, vol. 1. TENCON, 2003, pp. 300–304.
- [21] A. Girard and J.-S. Plante, "Applied control of binary robots based on influence vectors," in *International Conference on Robotics and Automation*. IEEE, 2013, pp. 523–529.
- [22] G. Miron, A. Girard, J.-S. Plante, and M. Lepage, "Design and manufacturing of embedded air-muscles for a magnetic resonance imaging compatible prostate cancer binary manipulator," *Journal of Mechanical Design*, vol. 135, no. 1, pp. 011 003–011 003, 2013.
- [23] W. Perruquetti and J.-P. Barbot, *Sliding Mode Control in Engineering*, 1st ed. CRC Press, 2002.